Ocean Engineering 281 (2023) 114736

Contents lists available at ScienceDirect

Ocean Engineering

journal homepage: www.elsevier.com/locate/oceaneng

# Comparison of different fidelity hydrodynamic-aerodynamic coupled simulation code on the 10 MW semi-submersible type floating offshore wind turbine

Ho-Seong Yang [a,*], Watchara Tongphong [a], Alkhabbaz Ali [c], Young-Ho Lee [b]

[a] Department of Mechanical Engineering, Korea Maritime and Ocean University, Busan, South Korea
[b] Division of Mechanical Engineering, Korea Maritime and Ocean University, Busan, South Korea
[c] Department of Aeronautical Technical Engineering, Technical College, AI-Kitlab University, Kirkuk, Iraq

ARTICLE INFO

Handling Editor: Prof. A.I. Incecik

*Keywords:*
Floating offshore wind turbine (FOWT)
Computational fluid dynamics (CFD)
Middle -fidelity simulation tool
10 MW-turbine
Semi-submersible system
Fully coupled simulation

ABSTRACT

This study aimed to analyze and examine the precision of a middle-fidelity simulation tool by performing load analysis using CFD and middle-fidelity analysis tools. The analysis was performed on a fully coupled system including turbine, platform, and mooring system under the severe operating state. Grid sensitivity tests were performed on the turbine and floater to increase the precision of CFD results. The results showed that the mid-fidelity analysis tool had a high error rate in surge and pitch load responses due to failure in considering the current load caused by wind. Moreover, potential flow-based analysis tools can be less accurate for complex-shaped structures such as the rectangular pontoon used in this study. To determine the extent to which the viscosity effect, dependent on the wet body shape, affects the accuracy of the results, this study compared the accuracy of potential flow-based analysis tools and CFD. This study contributes to the development of research in this field by providing new insights and undiscovered results for analyzing a FOWT with an unstructured shape.

## 1. Introduction

The global movement to transition from fossil fuels to renewable energy is rapidly on the increase. In 2021, the overall installed capacity for renew-able energy was 295 GW, with wind energy at 93.6 GW, making it the second largest capacity after PV (IEA, 2022). According to a GWEC (2021), by the end of 2021, the new capacity of wind power equipment is 72.5 GW for onshore and 21.1 GW for offshore, supplying 5.3% of the world's electricity demand. In the case of South Korea, the cumulative installed capacity as at the end of 2021 was 1.71 GW, and there are 109 wind power plants in operation nationwide. Comparing wind power generation costs, the global LCOE for onshore is $0.039/kWh and offshore is $0.084/kWh (IRENA, 2021). In Korea, onshore is $0.115/kWh and offshore is $0.230/kWh, showing that it is about three times higher than the world market. However, as the market expands, the LCOE price decreased by more than 50% compared to 10 years ago. In order to expand the wind power market and satisfy grid parity in Korea, R&D for floating offshore wind turbines and structures is being actively carried out. However, unlike fixed offshore wind power development, floating offshore wind power development requires not only wind turbine performance but also the performance of the sub-structure that sup-ports the wind power equipment, so it requires a lot of temporal and technological effort.

In the stage of researching and developing large-scale wind turbines, it takes a lot of time and development costs to make actual products, so product verification is performed in advance through scale model tests or simulation using engineering tools (Vorpahl et al., 2013; Ahlström, 2006; Wu and Porté-Agel, 2011; Bazilevs et al., 2011; Mihet-Popa et al., 2004; Hsu et al., 2014; Wang et al., 2012). Generally, in the case of onshore wind or fixed offshore wind, the fore-after movement of Nacelle due to external loads is not large. Therefore, even if low-fidelity engineering tools are used under the assumption that the shape characteristics are properly reflected, there is little difference between the actual calculation of thrust, torque, and output (Hansen et al., 2006). However, as the size of the turbine increases, deflection occurs in the spanwise and edgewise direction, and the values predicted by low-fidelity engineering tools differ from the actual performance of the turbine. To overcome this difference, various correction functions were added to increase the accuracy. Even though the accuracy is reduced at low speeds due to high tip speed ratio, the torque and output in the range from near the rated

* Corresponding author.
*E-mail address:* kpsc1908@g.kmou.ac.kr (H.-S. Yang).

https://doi.org/10.1016/j.oceaneng.2023.114736
Received 28 February 2023; Received in revised form 26 April 2023; Accepted 30 April 2023
Available online 20 May 2023

wind speed to cut-out wind speed can be well predicted with high accuracy considering the performance changes caused by the deflection of the turbine (Luna et al., 2022). By using such improved engineering tools and comparing the performance of floating wind turbines with high-fidelity engineering tools, it was observed that the results of engineering tools with different precisions fit perfectly when artificial pitching is given to the turbine (Ortolani et al., 2020).

To simulate a floating offshore wind system, both aerodynamic and hydrodynamic analysis must be performed simultaneously. Generally, middle-fidelity engineering tools perform hydrodynamic analysis through potential flow based numerical simulation (Bayati et al., 2015; Benitz et al., 2014, 2015; Robertson et al., 2014a,b; Ledru et al., 2014). Currently, the semi-submersible type used in the substructures of most floating offshore wind development systems has a surge and pitch natural frequency below the primary wave frequency range to avoid direct wave excitation. However, in actual seas, irregular waves with small non-linear low frequencies exist, and these waves can still cause pitch and sway resonance due to their excitation (Leimeister et al., 2018). The problem is that potential flow-based engineering tools mostly underpredict by more than 10% of the extreme and fatigue loads, and they have the largest underprediction rate in the low-frequency range (Robertson et al., 2017; Pegalajar-Jurado and Bredmose, 2019). Some researchers have performed research by reducing experimental uncertainties in the low-frequency response and distinguishing the components of loads to better understand the underprediction problem of potential flow-based hydrodynamic analysis tools (Robertson et al., 2017, 2020a; Pegalajar-Jurado and Bredmose, 2019). By adding a quadratic transfer function (QTF) and Morison element for wave excitation based on 2nd-order potential flow theory, the results were improved, but the predicted low-frequency response was different from the response measured in experiments. Additionally, the two added models predicted better results in fixed-state wave excitation and free-decay simulations compared to models without added drag and damping coefficients. However, they predicted worse results at the surge natural frequency (Robertson et al., 2020a).

On the other hand, high-fidelity engineering tools like Computational Fluid Dynamics (CFD) can correctly predict even the parts that low to middle-fidelity engineering tools cannot predict well, such as the prediction of difference-frequency wave excitation (Wang et al., 2021). Furthermore, experiments were also conducted to correct low to middle-fidelity engineering tools for hydrodynamic analysis, by comparing them with CFD (Tran and Kim, 2015). Unlike BEM method, CFD can accurately perform aerodynamic analysis without correction of analysis (Yang et al., 2014). Thus, by using CFD, it is possible to analyze the dynamic characteristics of FOWT in an environment that considers both the waves and the wind by fully-coupled simulation as it can accurately analyze hydrodynamic and aerodynamic phenomena simultaneously. Tran and Kim (2018) have performed fully coupled analysis using CFD by combining NREL 5 MW turbine and OC4-Semi submersible platform. In this research, to validate the CFD technique, a comparison was made with the middle-fidelity engineering tool, FAST and it was observed that the two tools showed relatively good correlation in both the aerodynamic side and the prediction of platform motion in the 6-DoF moving system. Zhou et al. (2021) performed simulation of coupled aero-hydro mooring FOWT using CFD to analyze the wave type and steep slope effects on hydro/aerodynamics. Through this study, it was confirmed that the wave type or steep slope has little effect on the aerodynamic performance of FOWT.

While middle-fidelity engineering tools underpredict the movement of the substructure due to waves in hydrodynamic analysis, they are capable of performing aerodynamic analysis at a similar level as high-fidelity engineering tools (Hansen et al., 2006; Luna et al., 2022; Ortolani et al., 2020). Through the abovementioned studies, it is believed that there is little difference between middle-fidelity engineering tools and high-fidelity engineering tools, CFD in terms of predicting the overall turbine thrust and output. However, there is a lack of sufficient research available for using middle-fidelity engineering tools depending on the size of the turbine as well as the shape and characteristics of the floater. Most current FOWT research involving semi-submersible floaters uses the 5 MW DeepCwind floater, which consists of all parts in a cylindrical shape and is capable of applying viscous effects with high accuracy in potential flow-based analysis tools. However, there is a relative dearth of reference and research for floaters with shapes that make it difficult to accurately apply viscous effects. Therefore, the creation of related references and additional validation studies are needed.

This paper describes the analysis of the error between engineering tools with different precisions using high-fidelity engineering tool, Star-CCM+ and a middle-fidelity engineering tool, OrcaFlex for a 10 MW turbine applied to a FOWT. In this study, we used a floater with a rectangular pontoon at the bottom to analyze the error rate of middle-fidelity engineering tool for unstructured substructures, which found it difficult to implement accurate viscous effects that were not well-performed in previous research. The analysis includes not only the movement of the platform, but also the tension applied to the fairlead. Critical conditions of the operating environment were applied, and a large wind turbine, the DTU 10 MW wind turbine, was applied as the turbine. Additionally, a newly designed tower, floater, and mooring line were used to apply the 10 MW turbine.

## 2. Methodology

In order to analyze errors between programs with different precisions, it is necessary to understand the differences in the theories used. The analysis is mainly divided into three parts: aerodynamic, hydrodynamic, and mooring. The high-fidelity engineering tool, Star-CCM+ and the middle-fidelity analysis tool, OrcaFlex which can perform aerodynamic-hydrodynamic-mooring analysis at once, were used for interpretation. The core parts of the theory applied to each program are explained below.

### 2.1. OrcaFlex

#### 2.1.1. Aerodynamics

In OrcaFlex, the Blade Element Momentum Theory (BEMT) is used for aerodynamic analysis (Moriarty and Hansen, 2005). BEM theory assumes that the blades are composed of several independent elements. Each independent element contains aerodynamic information such as lift and drag coefficients based on a 2D airfoil shape, and moment coefficients to calculate the load on the blade. Unlike CFD, BEM method does not require formation of the blade shape or the grid in the surrounding area of the blade in order to calculate the load on the blade. By repetitively performing calculations based on Blade Element theory and Momentum theory, the BEM can simply and accurately calculate the thrust or output of the turbine. BEM theory can be considered a 2D theory that is based on the rotating plane of the frame. The flow in the span direction is ignored. As a result, the accuracy of the calculation is lowered due to the lack of proper implementation of hub loss, tip loss, and skewed inflow caused by the flow direction in the span direction. To compensate for these defects, Prandtl's theory, represented by equation (1), is reflected in the BEM equation by incorporating the velocity field F. Equations (2) and (3) represent correction functions to be included in equation (1), and when calculating tip loss, equation (2) is applied to calculate the velocity field for tip loss, and when calculating hub loss, equation (3) is applied to equation (1) to calculate the velocity field. Here, B represents the number of blades, R represents the rotor radius, r represents the local radius, and $\varphi$ represents local inflow.

$$F = \frac{2}{\pi} cos^{-1} e^{-f_{tip}} \tag{1}$$

$$f_{tip} = \frac{B}{2} \frac{R - r}{r sin\varphi} \text{ If tip loss is consider} \tag{2}$$

$$f_{tip} = 1 \text{ If tip loss is not considered} \tag{3}$$

The BEM theory was designed with the assumption of axisymmetric flow, so in situations where the rotation axis and the direction of the wind of-ten do not match, such as for floating wind power devices, the accuracy of predicting the Skewed wake effect that occurs behind the rotor is significantly reduced. This skewed wake also affects the output or thrust of the turbine, so accurate interpretation requires correction, and Glauert has developed equations to correct the wake (Glauert, 1926). In this study, we used the wake correction model derived from the Glauert model developed by Pitt and Peters, as shown in Fig. 1, and corrected the wake through equation (4) where $\chi$ represents the segment azimuth angle, $\psi$ is the rotor wake angle.

$$a_{skew} = a\left[1 + \frac{15\pi}{32}\frac{r}{R}tan\frac{\chi}{2}sin\,\psi\right] \tag{4}$$

### 2.1.2. Hydrodynamics

For hydrodynamics analysis, potential flow theory is applied. Potential flow can be defined as a representation of the velocity field being a gradient of a scalar function. Fluid field that are analyzed by potential flow have the characteristic that the curl of the scalar gradient is always zero, meaning that they are non-rotational. In fluid dynamics, potential flow is defined as a function of time and space, known as the velocity potential, $\varphi$. The fluid velocity $V$ is a vector field defined by the gradient, $\nabla$ of the velocity potential, as shown in equation (5). By vector calculus, the gradient of curl is also 0, as shown in equation (6), therefore, the curl of the velocity field is also 0.

$$V = \nabla\varphi \tag{5}$$

$$\nabla \times \nabla\varphi = 0 \tag{6}$$

This means that, as mentioned above, the potential flow theory is a non-rotational flow. Therefore, it is not suitable for predicting strong vortices or boundary layers, but it can be applied to the analysis of cases where non-rotational flows such as external flow of a wing or plane, wave flow, etc. are dominant. Potential flow theory is used absolutely in the analysis of ships and marine structures because it can implement waves like actual fluid with simple equations. However, it has a limitation whereby it cannot reflect the influence of viscosity and vorticity of the fluid because it is assumed that the flow of the fluid is non-viscous and non-rotational. Therefore, when the flow above has a significant influence on the motion, there is a difference between realities, and the characteristics of the object are analyzed to reflect the viscosity effect, but there are some limitations in perfectly implementing the actual movement (Robertson et al., 2020).

In this study, the OrcaWave program, a wave analysis software that calculates the load and response of wetted bodies due to surface waves using potential flow theory, was utilized to estimate several crucial parameters. These parameters include Displacement RAO (Response Amplitude Operator), Load RAO, Wave Drift RAO, Added Mass, and Additional Damping. The results obtained from the OrcaWave program were inputted into the OrcaFlex program, where they were utilized for the hydrodynamic analysis required for integrated load analysis.

### 2.1.3. Mooring lines

In the middle-fidelity engineering tool, the mooring line is implemented using the lumped-mass approach and it is applied to the analysis (Hall and Goupee, 2015). The mooring line is divided evenly into n lines, as shown in Fig. 2, forming n+1 nodes that include the anchor position and fairlead position. Properties such as unstretched length, volume equivalent diameter, density, Young's modulus, and damping coefficient are assigned to the segmented line, located in the middle of each node, $l_{i+1/2}$. Based on the node, information such as load, force, and weight that is applied to the segmented line on both sides is received at the node and calculated as shown in Fig. 3. Through these calculations of forces at each node, the loads on the mooring shape, anchor, and fairlead can be predicted.

## 2.2. Star-CCM+

### 2.2.1. Aerodynamics

The high-fidelity engineering tool, CFD, does not require correction functions for accurate aerodynamic analysis, unlike BEM theory. CFD analyzes the 3-dimensional fluid dynamics area by dividing it into countless small volumes, and solving the Navier-stokes equation, which mathematically calculates the energy, mass, and pressure information of each volume based on the conservation laws of fluid dynamics. At this time, CFD applies turbulence theory to model the complex interactions of actual fluid flow. Turbulence modeling typically involves methods such as RANS (Reynolds Averaged Navier-Stokes), LES (Large Eddy Simulation), and DNS (Direct Numerical Simulation). In practice, applying the DNS model in CFD is challenging due to several reasons. First, DNS requires extremely fine spatial and temporal resolutions to resolve all scales of turbulence, which leads to an enormous computational cost. This makes it infeasible for most industrial applications where computational resources are limited. Second, the complexity of the geometry and boundary conditions in real-life situations often makes it difficult to implement DNS accurately. As a result, alternative turbulence modeling approaches such as RANS and LES are more commonly used in CFD, as they offer a balance between accuracy and computational efficiency. Krogstad and Eriksen (2013) analyzed turbine performance using various types of turbulence models, such as RANS models like k-epsilon and SST (Shear Stress Transport), as well as LES models. They found that overall, most of these methods were able to predict power production and thrust quite accurately under operational conditions.

RANS-based models require significantly less computational

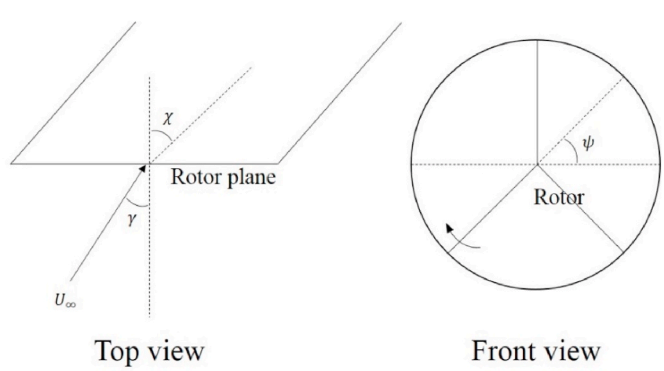


**Fig. 1.** Coordinates used in skewed wake correction (Moriarty and Hansen, 2005).

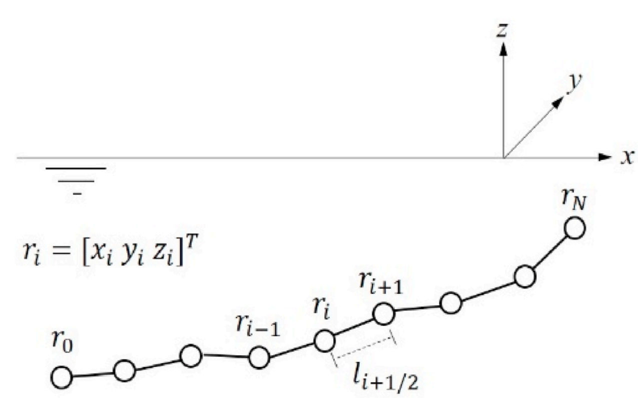


**Fig. 2.** Discretized mooring line schematic in OrcaFlex.

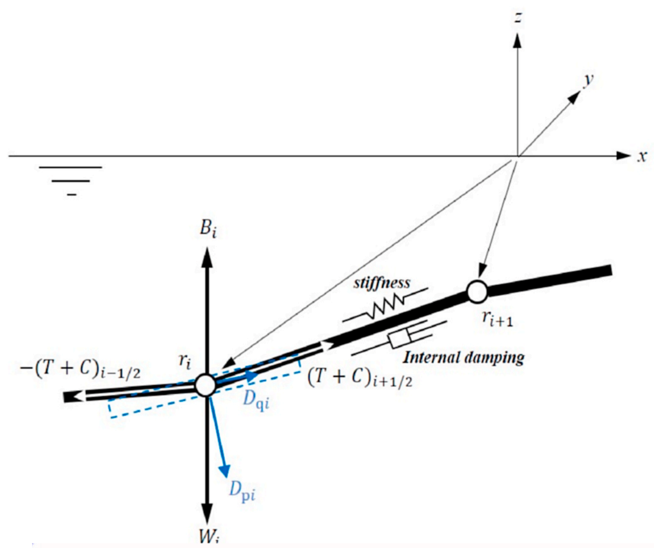


**Fig. 3.** Cable forces induced by internal/external forces in OrcaFlex.

resources compared to LES, as they model the entire range of turbulent scales, while LES resolves the larger scales and models the smaller scales only. This makes RANS more efficient for complex and large-scale simulations, such as those involving FOWT. So, in this search, we applied the k-Omega SST (menter) turbulence RANS model, which combines the equations of the k-Omega and k-Epsilon models using a weighting function, to more accurately simulate the turbulence in the domain.

The Navier-stokes equation is defined as a governing equation by the laws of mass conservation, momentum conservation, and energy conservation, represented by equations (7) and (8). Here, $u$ represents fluid velocity, total pressure, $p$, gravitational acceleration, $g$, the coefficient of pressure, $\mu$ and density, $\rho$. Additionally, temperature changes of fluid are not a dominant factor in this research, so the energy conservation law is ignored.

Continuity equation:

$$\frac{\partial\rho}{\partial t}+\frac{\partial}{\partial x_i}(\rho u_j)=0 \tag{7}$$

Momentum equation:

$$\frac{\partial\rho}{\partial t}(\rho u_i)+\frac{\partial}{\partial x_j}(\rho u_i u_j)=\frac{\partial}{\partial x_j}\left[-p\delta_{ij}+u\left(\frac{\partial u_i}{\partial x_j}+\frac{\partial u_j}{\partial x_i}\right)\right]+\rho g_i \tag{8}$$

### 2.2.2. Hydrodynamics

CFD, like aerodynamic analysis, solves Navier-Stokes equations considering mass and momentum conservation laws to perform a hydrodynamic analysis. In this study, a Volume of Fluid (VoF) multiphase model was applied to perform the analysis where two phases exist in the fluid domain. VoF is an interface capturing a method that predicts the distribution and movement of non-homogeneous interfaces and is assumed to be suitable for resolving the position and shape of the interface between the phases with appropriate mesh resolution. Therefore, the volume of fraction of the phase is defined by the following equation (9).

$$a_i=\frac{V_i}{V} \tag{9}$$

Here, $V_i$ refers to the volume of phase $I$ and $V$ refers to the volume of the cell. In this study, we applied two phases (air, water) so the volume of fraction is defined as shown in equation (10).

$$a_{i.water}+a_{i.air}=1 \tag{10}$$

At this time, if $a_i$ is 0, it means state i is completely void in the cell, and if $a_i$ is 1, it means state i is completely filled in the cell. As a result, the two separated fluids in the cell have their own corresponding densities and viscosities, etc., and Navier-stokes equation is solved. Floating wind turbine is not a rotating form on a fixed axis, but it rotates on a moving platform, so Dynamic Fluid-Body Interaction (DFBI) is used to predict the 6DoF movement of the floating object on water (Ohmori, 1998; Shabana, 2001). To apply DFBI, the center of gravity, moment of inertia, and other additional moments generated by the rotation of the turbine and other external forces and momentum elements are set for the FOWT system, and the set values are reflected in the system with other external forces as shown in the following equation (11)(12) (CD-ADAPCO, 2020).

$$F=f_r\sum f+\sum f_c \tag{11}$$

$$F=f_r\sum n+\sum n_c \tag{12}$$

Here, F and N represent the total force and momentum applied to the object, $f_c$ represents the external forces generated by the multibody constraint, f represents all other forces such as fluid, gravity, and user-defined forces, $n_c$ represents the external momentum generated by the multi-body constraint, n represents all other momentums such as fluid, gravity, and user-defined momentum. $f_r$ is a time-ramping function that is determined by the user-specified release time and ramp time.

### 2.2.3. Mooring lines

In CFD, in order to moor FOWT to the Seabed, a flexible, quasi-fixed catenary is applied between two endpoints which are affected by its own weight in the gravitational field. The shape of the catenary is given by the following equation (13) in a local cartesian coordinate system (CD-ADAPCO, 2020).

$$x=au+b\sinh(u)+\alpha$$

$$y=a\cosh(u)+\frac{b}{2}\sinh^2(u)+\beta \tag{13}$$

$$\text{for } u_1\le u\le u_2$$

Here,

$$a=\frac{c}{\lambda_0 g}$$

$$b=\frac{ca}{DL_{eq}}$$

$$c=\frac{\lambda_0 L_{eq} g}{\sinh(u_2)-\sinh(u_1)}$$

In the above equation, $g$ represents gravitational acceleration, $\lambda_0$ and $L_{eq}$ represents the unit mass per unit length and the relaxation length, $D$ represents the strength of the catenary, and $\alpha$ and $\beta$ is an integration constant that depends on the endpoints $u_1$ and $u_2$ and the overall mass. Here, the curve parameter $u$ is described through the inclination angle of the catenary curve using the following equation (14) (CD-ADAPCO, 2020).

$$tan\ \varphi=sinh\ (u) \tag{14}$$

So, when the weight, length, strength, and values that are set are reflected and the shape of the catenary is determined, a force similar to Fig. 4 is applied at both ends of the catenary, and f is simply given by (equations (15) (16).

$$f_{1,x}=c$$

$$f_{1,y}=c\sinh(u_1) \tag{15}$$

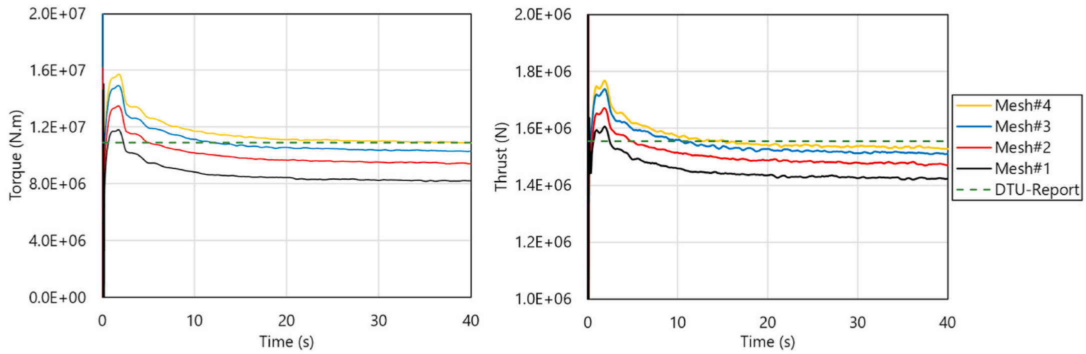


**Fig. 8.** Turbine mesh sensitivity result (torque, thrust).

**Table 4**
Turbine mesh sensitivity error comparison.

| Case | Mesh #1 | Mesh #2 | Mesh #3 | Mesh #4 |
|---|---|---|---|---|
| Thrust (N) | 1,421,310 | 1,468,817 | 1,505,372 | 1,525,293 |
| Torque (N-m) | 8,161,058 | 9,355,822 | 10,196,653 | 10,809,480 |
| Thr. error (%) | 8.60% | 5.54% | 3.19% | 1.91% |
| Tor. error (%) | 25.17% | 14.22% | 6.51% | 0.89% |

**Table 5**
Platform mesh sensitivity simulation condition.

| Parameters | Value |
|---|---|
| Simulation method | Unsteady |
| Turbulence model | K-omega SST (menter) |
| Free surface model | Volume of Fluid (VoF) |
| Wave model | Regular wave |
| Wave height | 8.12 m |
| Wave period | 13.0 s |
| Wind speed | N/A |
| Water density | 1025 kg/m$^3$ |
| Air density | 1.225 kg/m$^3$ |
| Water depth | 150 m |
| Mooring method | Catenary |

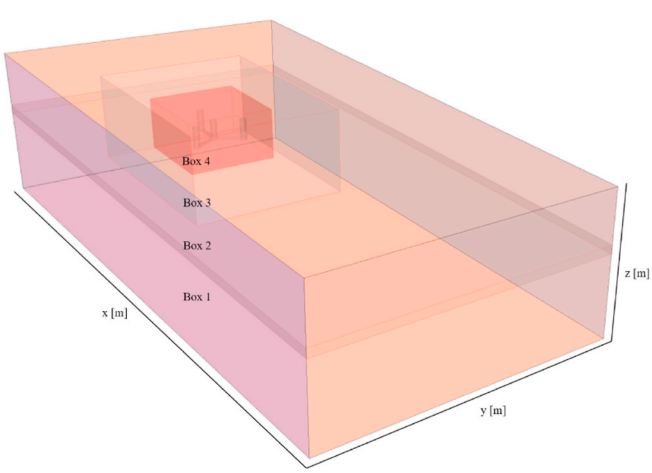


**Fig. 9.** Refinement zone division for platform mesh sensitivity analysis.

side, from Mesh #1 with large grid size to Mesh #4 with dense grid size, and the water vorticity scene at Z = 0 m viewed from above to confirm the water surface resolution. Looking at the water vorticity at that level, vorticity was not properly implemented in the gradient area behind the waves due to the low resolution in Mesh #1 and Mesh #2. On the other hand, from Mesh #3, vorticity was implemented more accurately in the gradient area behind the waves. Fig. 12 shows a graph of the representative motion response of the floating body in time series, representing the response characteristics for surge, pitch, and heave from left to right. To have a regular movement in surge and pitch, more analysis is required, but it was sufficient for the sensitivity test. In the pitch movement, there was almost no response error according to the grid size, but from 300s to 350s, it was confirmed that the platform tended to respond insufficiently with a lower grid resolution in the surge and heave responses.

Tables 8–10 were used to numerically analyze the response errors of the buoyancy structure according to the grid size, summarizing the maximum, minimum, and average values of the buoyancy motion in a table format. Table 6 shows the results of the grid sensitivity analysis for surge motion. It can be seen that as the grid resolution increases, the error in the maximum, minimum, and average values decreases, and from Mesh #3, the average error decreases to around 10%. Table 7 shows that the grid sensitivity for pitch motion resulted in response error rates of 5% or less regardless of the grid resolution. Table 8 shows the response error due to the grid resolution for heave motion, where the error rate decreases as the resolution increases, and from Mesh #2, the average error rate decreases to around 10%. Therefore, the grid structure of Mesh #3, which showed an overall average response error of about 10%, was applied to the substructure grid structure in the integrated load analysis.

## 4. Fully coupled simulation

After performing a grid sensitivity analysis, preparations were made for analysis of the motion and load response error rates of the floating wind turbine system according to precision. To perform the analysis, preparations for interpretation were made for each program, as shown in Fig. 13. All programs used in the analysis modeled the turbine, tower, floating body, and mooring lines.

The turbine used for the analysis was designed to have a straight blade at wind speed close to 11 m/s. The same rotor with straight blades used in the grid sensitivity test was applied. The overall characteristics of the turbine size and components are shown in Table 11. The hub was located 118.38 m above sea level and 7.07 m away from the tower center. A tilt angle of 5° was considered in this analysis, resulting in a hub height of 119.37 m and a displacement of 7.043 m from the tower center.

Regarding the tower that makes up the floating offshore wind power plant, it was designed to have a bottom diameter of 9 m, top diameter of 5.5 m, length of 98.13 m, and weight of 655 tons at a height of 17.5 m from MSL, as shown in Table 12. It was designed considering safety and elasticity, but in the error analysis according to the precision of the analysis, it was assumed as a rigid body that does not buckle. The 10 MW semi-submersible platform designed as shown in Fig. 14 was used for the analysis. The platform was designed with a total length of 32 m, pontoon

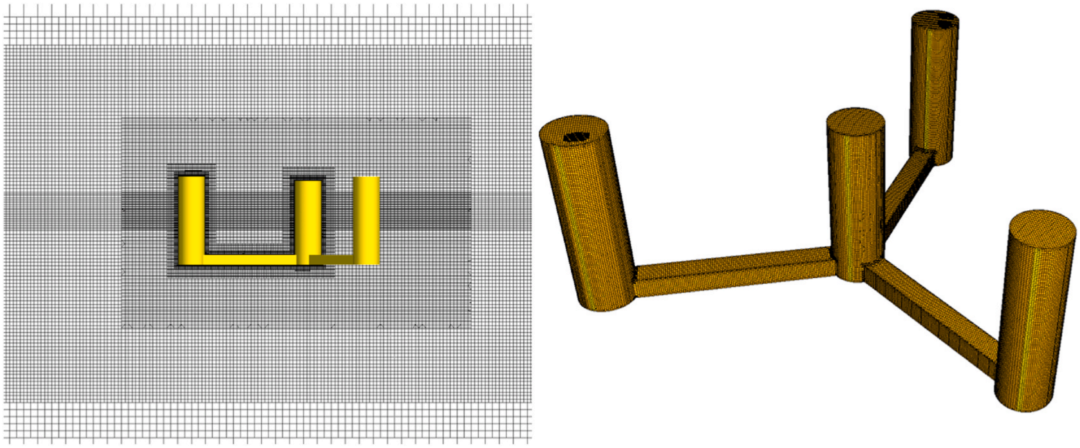

**Fig. 10.** Platform overall region and surface mesh grid composition.

**Table 6**
Refinement zone information – platform mesh sensitivity analysis.

| Case | x [m] | y [m] | z [m] | $\Delta l_x/S_{platform}$ | $\Delta l_y/S_{platform}$ | $\Delta l_z/S_{platform}$ | Mesh type |
|---|---|---|---|---|---|---|---|
| Box 1 | [-250, 750] | [-250, 250] | [-150, 100] | 40 | 40 | 40 | Trim (isotropic) |
| Box 2 | [-250, 750] | [-250, 250] | [-7.5, 7.5] | 10 | 10 | 5 | Trim (Anisotropic) |
| Box 3 | [-150, 200] | [-130, 130] | [-80, 70] | 10 | 10 | 10 | Trim (isotropic) |
| Box 4 | [-80, 70] | [-75, 75] | [-50, 40] | 10 | 10 | 10 | Trim (isotropic) |

**Table 7**
Number of cell, platform boundary layer cell setting information.

| Case | Mesh #1 | Mesh #2 | Mesh #3 | Mesh #4 |
|---|---|---|---|---|
| Platform surface | 0.3 m | 0.25 m | 0.2 m | 0.15 m |
| First layer thickness | 0.5 mm | 0.5 mm | 0.5 mm | 0.5 mm |
| Number of layer | 10 | 10 | 10 | 10 |
| Background area number of mesh | 1,484,700 | 2,534,963 | 4,523,440 | 10,050,536 |
| Overset region area number of mesh | 493,102 | 689,975 | 1,111,919 | 1,961,793 |

width of 8 m, height of 4.8 m, outer column diameter of 12 m, and tower column diameter of 9 m. The weight center and inertial moment were determined considering the static balance and stability of the platform, as shown in Table 13.

The semi-submersible platform was designed to maintain its position using a three-point mooring system that applies the catenary method by connecting the chains. The characteristics of the mooring lines, anchor, and fairlead positions are shown in Table 14. The length of the lines was de-signed to be 850 m, the weight per unit length was 162.51 kg, and the axial stiffness was 2710 kN/m. Although, the actual weight per unit length of the designed mooring line is 430.019 kg (dry)/346.7 kg (wet), in the CFD, it was set as a single weight because there are limitations in distinguishing the mooring line into wet and dry parts. In this case, the total weight was divided by the length of the mooring line, excluding the part where the mooring line was anchored to the bot-tom when the system achieved static balance, to determine the single weight.

The simulation analysis conditions were set up as shown in Fig. 15. The left side of the figure shows the boundary conditions for performing CFD simulation using Star-CCM+, while the right side shows the boundary conditions of the OrcaFlex. In CFD, the overset region was set as overset mesh to allow the system to move freely in 6 degrees of freedom. For the fully coupled simulation, the reference coordinates of the rotating region were constrained to the overset region containing the platform and tower, enabling the turbine to undergo rotational motion, and simultaneously reflecting the 6 degrees of freedom movement of the system. The environmental and constraint conditions applied throughout these analysis processes can be found in Table 15. For fully-coupled simulation, unsteady simulation method and 0.05s time step was used. The wave spectrum used was the regular wave Airy, with a

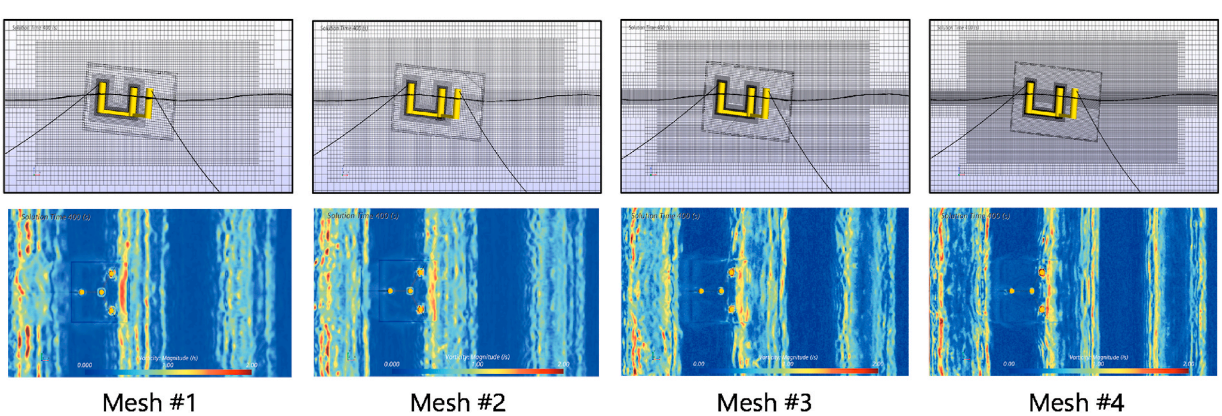


**Fig. 11.** Platform mesh sensitivity analysis vorticity result (t = 400s).

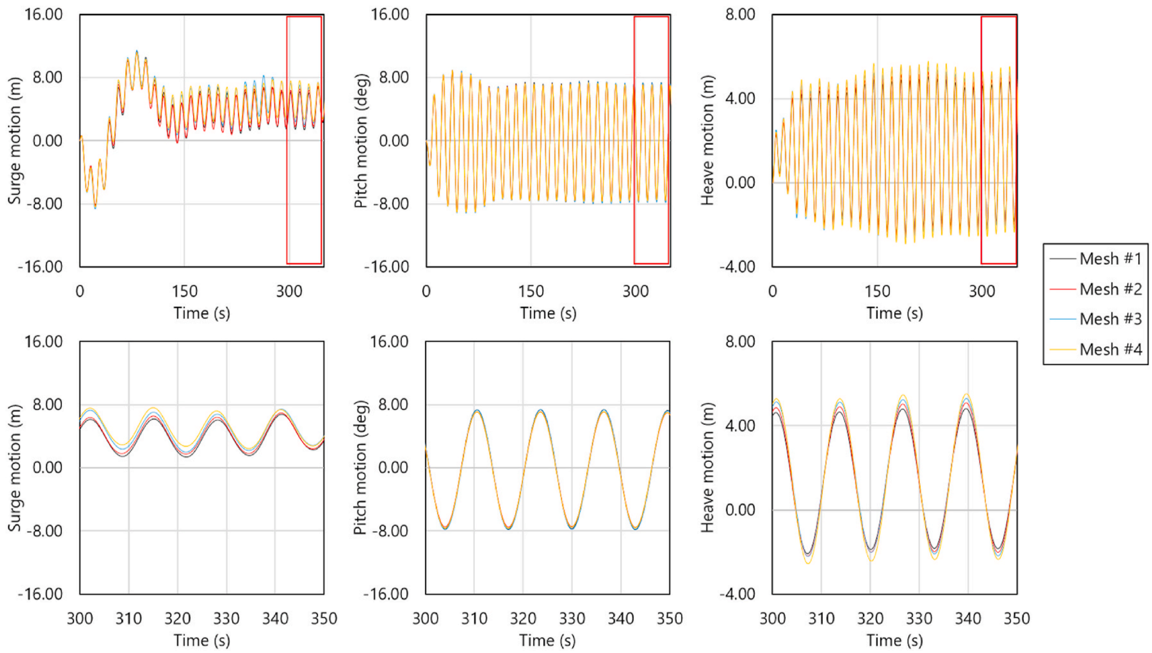


**Fig. 12.** Platform mesh sensitivity analysis result (left: surge, middle: pitch, right: heave).

**Table 8**
Platform mesh sensitivity analysis simulation result–surge motion.

| Parameters | Mesh Size | | | |
|---|---|---|---|---|
| Output | Mesh #1 | Mesh #2 | Mesh #3 | Mesh #4 |
| Average (m) | 3.901 | 4.135 | 4.634 | 4.957 |
| Minimum (m) | 1.381 | 1.750 | 1.991 | 2.433 |
| Maximum (m) | 6.777 | 6.943 | 7.427 | 7.618 |
| Avg. error (%) | 21.31% | 16.57% | 6.51% | – |
| Min. error (%) | 43.24% | 28.07% | 18.17% | – |
| Max. error (%) | 11.03% | 8.86% | 2.51% | – |

**Table 9**
Platform mesh sensitivity analysis simulation result-pitch motion.

| Parameters | Mesh Size | | | |
|---|---|---|---|---|
| Output | Mesh #1 | Mesh #2 | Mesh #3 | Mesh #4 |
| Average (m) | 4.783 | 4.615 | 4.807 | 4.657 |
| Minimum (m) | −7.785 | −7.538 | −7.842 | −7.635 |
| Maximum (m) | 7.371 | 7.090 | 7.385 | 7.106 |
| Avg. error (%) | 2.71% | 0.90% | 3.23% | – |
| Min. error (%) | 1.96% | 1.27% | 2.71% | – |
| Max. error (%) | 3.73% | 0.23% | 3.93% | – |

**Table 10**
Platform mesh sensitivity analysis simulation result-heave motion.

| Parameters | Mesh Size | | | |
|---|---|---|---|---|
| Output | Mesh #1 | Mesh #2 | Mesh #3 | Mesh #4 |
| Average (m) | 2.116 | 2.242 | 2.336 | 2.490 |
| Minimum (m) | −2.075 | −2.192 | −2.210 | −2.553 |
| Maximum (m) | 4.810 | 5.087 | 5.290 | 5.521 |
| Avg. error (%) | 15.02% | 9.96% | 6.15% | – |
| Min. error (%) | 18.72% | 14.13% | 13.46% | – |
| Max. error (%) | 12.88% | 7.86% | 4.19% | – |

wave height of 6 m and a period of 10s, based on the study by Robertson et al. (2014a,b). The wind speed was assumed to be uniformly 11 m/s, which is rated wind speed of turbine, throughout the entire area, with the wind and wave directions acting in the same direction as the turbine's heading. For the restraint conditions, a straight-shaped turbine was used instead of a pre-bend shape, and a rigid body without elastic dynamics was applied. The RPM was set at 8.836, which is suitable for the corresponding wind speed. As the CFD could not reflect the touch-down effect of the anchor line, the water depth was adjusted to prevent the touch-down effect from being reflected in the middle-fidelity.

## 5. Results

The simulation error rates of the Star-CCM+ and OrcaFlex are as follows. Fig. 16 shows the time series of torque and thrust obtained by performing fully-coupled FOWT analysis using the middle-fidelity engineering tool, OrcaFlex and the high-fidelity engineering tool, CFD. Although the periods are the same, there is a slight phase difference in both torque and thrust due to the unsynchronized wave starting points of the two programs. One of the OrcaFlex analysis results was performed at IHU (Inha University), and an error analysis was performed with the results provided by IHU. Looking at torque in Table 16, both the middle-fidelity engineering tool and the high-fidelity engineering tool showed an average torque of around 10,000 kN-m. The middle-fidelity engineering tool showed a maximum error of within 15% relative to CFD, which was used as the reference. About 10% error occurred between the same programs, which was confirmed to have occurred during the process of inputting the DTU 10 MW turbine information into the program. As for the thrust, the values were generally around 1500 kN, and a maximum error of within 7% was confirmed.

Figs. 17 and 18 show the time serial response and power spectral densities. Table 17 presents the CFD and OrcaFlex results and errors for the motion response of the system. Analyzing from Surge, unlike the performance results of the turbine, the two OrcaFlex results were almost predicted identically. However, when compared with CFD, the motion response showed a result that was underestimated by an average of about 5 m. The middle-fidelity engineering tool has a limit of underestimating motion in the low-frequency range if it does not consider additional factors such as drag due to fluid separation on the platform. However, the environmental conditions in which the simulation was performed this time were closer to the high-frequency range than the

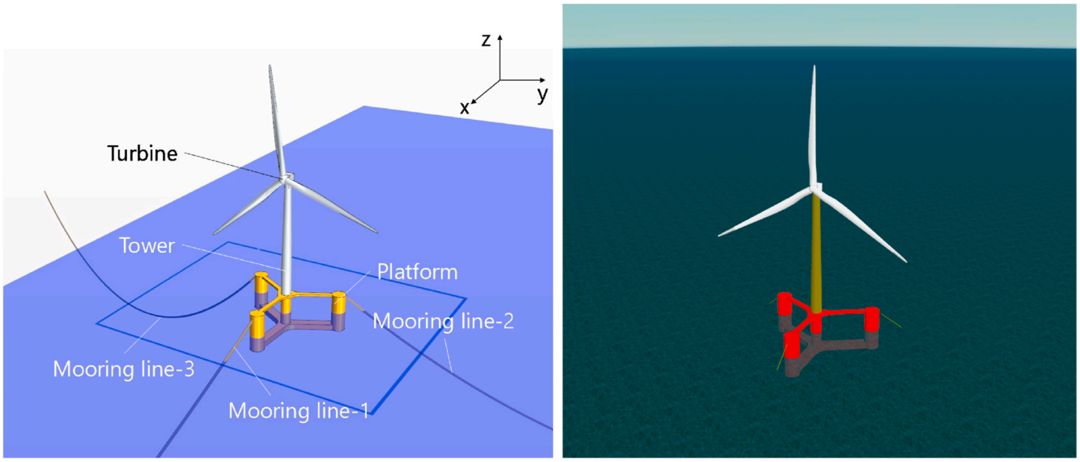


**Fig. 13.** Fully coupled simulation set-up (left: CFD, right: Middle-fidelity code.

**Table 11**
Turbine properties.

| Parameters | Value |
|---|---|
| Rated power | 10 MW |
| Rated wind speed | 11.4 m/s |
| Rated rpm | 9.6 |
| Rotor diameter | 178.3 m |
| Hub diameter | 5.6 m |
| Hub height (consider tilt) | 119.37 m |
| Hub position (from tower center/consider tilt) | 7.043 m |
| Tilt angle | 5 deg |

**Table 12**
Tower properties.

| Parameters | Value |
|---|---|
| Tower bottom position (from MSL) | 17.5 m |
| Tower bottom diameter | 9 m |
| Tower top diameter | 5.5 m |
| Tower length | 98.13 m |
| Tower Weight | 655 ton |

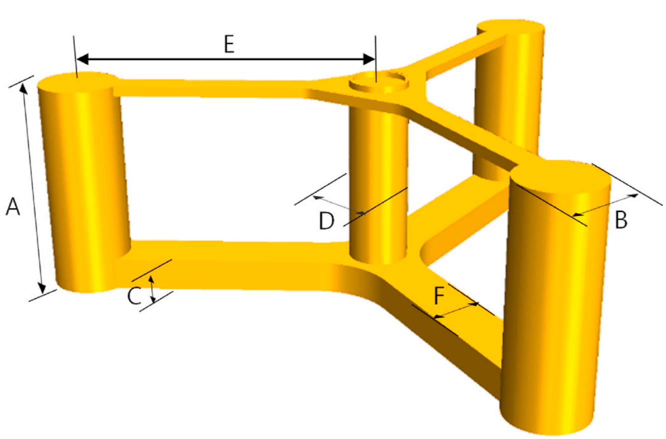


**Fig. 14.** 10 MW Semi-submersible platform.

low-frequency range, so this reason is not the cause of the error, and the error of the CFD and high-fidelity engineering tools is judged to be caused by the current in this analysis. In CFD, a current was generated in the area near the sea surface due to the wind, and this current applied a load to the platform, causing a difference in the platform's movement. In

**Table 13**
Platform properties.

| Parameters | Value |
|---|---|
| Platform geometry | |
| Platform height (A) | 32 m |
| Outer column diameter (B) | 12 m |
| Pontoon height (C) | 4.8 m |
| Tower column diameter (D) | 9 m |
| Column span (E) | 45 m |
| Pontoon width (F) | 8 m |
| Platform properties | |
| Weight (including tower, RNA only) | 10,254 ton |
| Center of mass (from SWL) | −0.04, 0, 4.185 m |
| Moment of inertia (from CoM) | 1.9672e7, 1.9612e7, 1.298e7 ton-m2 |

**Table 14**
Mooring properties.

| Parameters | Value |
|---|---|
| Mooring properties | |
| Unit length | 162.51 kg/m |
| Unstretched length | 850 m |
| axial stiffness | 2710 kN/m |
| Anchor position (from MSL) | |
| Mooring 1 | 852.69, 0, −150 m |
| Mooring 2 | −426.35, 738.45, −150 m |
| Mooring 3 | −426.35, −738.45, −150 m |
| Fairlead position (from MSL) | |
| Mooring 1 | 52.73, 0, 8.895 m |
| Mooring 2 | 26.305, 45.631, 8.895 m |
| Mooring 3 | 26.305, −45.631, 8.895 m |

the case of heave, the effect of the current is small due to the up and down motion, so the motion response error between CFD and OrcaFlex is shown to be within 1% in both the graph and table. However, there was a slight difference in the average heave value between the OrcaFlex results. This is due to the difference in weight settings of about 400 tons in IHU when inputting the platform hydrodynamics into OrcaFlex, and if this is taken into consideration, the phase and amplitude of the heave movement of the platform is performed by the two organizations using OrcaFlex match. The pitch showed a large error of about 30% in motion response between CFD and OrcaFlex because the load due to the current was not considered, similar to surge. Except the phase mean value, three simulation results have a good correlation with FOWT frequency response.

Fig. 19 shows the velocity response of the platform according to the

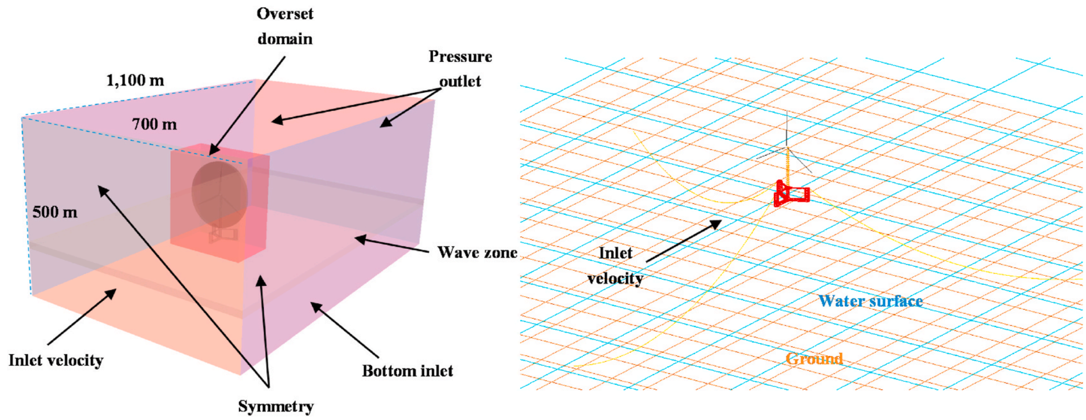


**Fig. 15.** 10 MW FOWT simulation boundary condition (left: CFD, right: Middle fidelity code).

**Table 15**
Simulation environment & operation condition.

| Parameters | Value |
|---|---|
| Environment condition | |
| Wave spectrum | Airy |
| Wave period | 10 s |
| Wave height | 6 m |
| Wind spectrum | constant |
| Wind velocity | 11 m/s |
| Wind & Wave direction | Alignment |
| Constraint condition | |
| RPM | 8.836 |
| Blade state | Rigid/Straight |
| Mooring state | No-touch down |

time series. Considering the surge and heave velocity response from left to right, as in the motion response, the analysis between OrcaFlex shows that they are consistent. However, due to the influence of the current, CFD showed a slightly higher amplitude than the middle-fidelity engineering tool, and although the phase between OrcaFlex analysis results was the same for pitch, a slightly higher amplitude was observed in CFD.

Here, the velocity amplitude was slightly lower in the IHU OrcaFlex results than in the results performed at KMOU, which is judged to be an error caused by applying a center of gravity 0.35 m higher at IHU. As shown in Table 18, when numerically analyzing the error rate, compared to CFD, the surge speed response error was about 17%, heave was within 1%, and pitch was an average of about 32%. In the surge and pitch speed response, there was a slight difference in the error between CFD and the OrcaFlex due to the current. Looking at the acceleration response of the plat-form in Fig. 20 and the graph in Table 19, the acceleration amplitude in the surge acceleration response is 16.64% for KMOU and 17.72% for IHU, and both middle-fidelity engineering tools showed errors that were almost consistent with those in the velocity

**Table 16**
Different fidelity tools result of the fully-coupled simulation (torque, thrust).

| Parameters | | OrcaFlex (KMOU) | Orcaflex (IHU) | CFD |
|---|---|---|---|---|
| Torque | Mean [kN-m] | 10,581 | 9611 | 9202 |
| | Mean. error [%] | 14.99% | 4.45% | – |
| Thrust | Mean [kN] | 1528 | 1468 | 1429 |
| | Mean. error [%] | 6.94% | 2.79% | – |

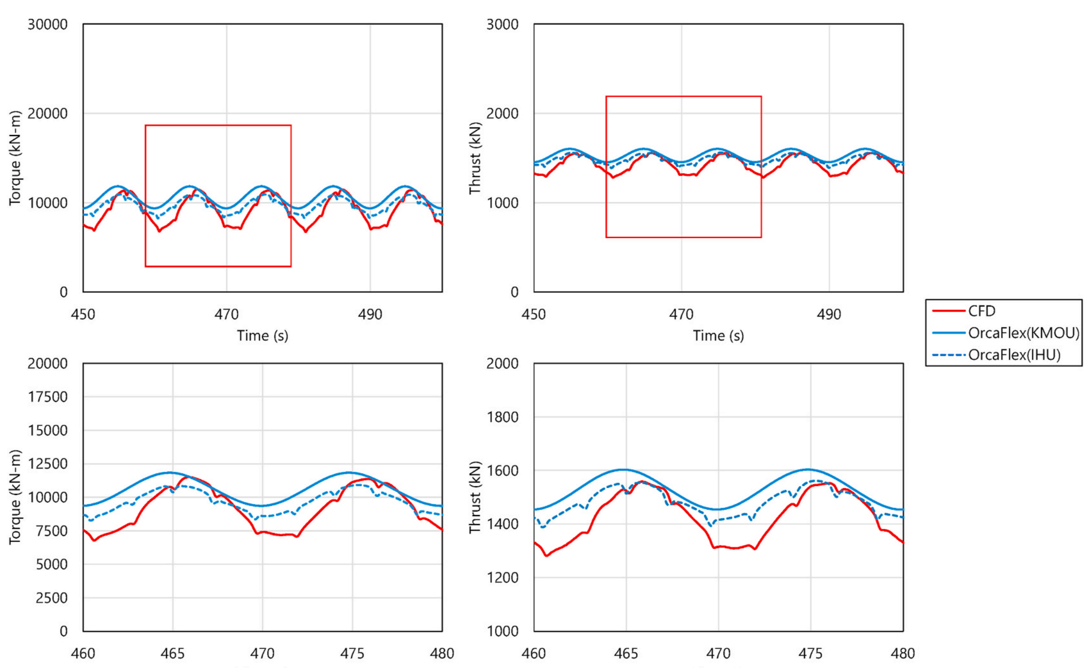


**Fig. 16.** FOWT simulation time serial result (left: torque, right: thrust).

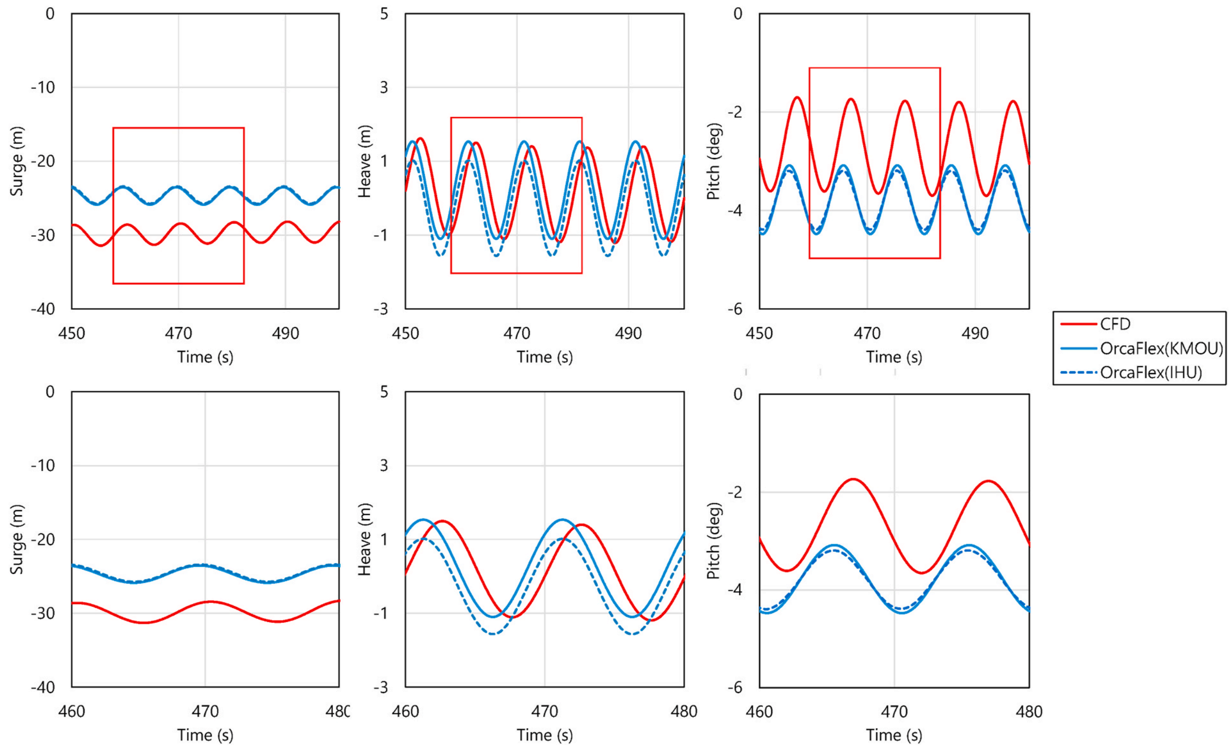


**Fig. 17.** FOWT simulation time serial displacement response result (left: heave, middle: pitch, right: surge).

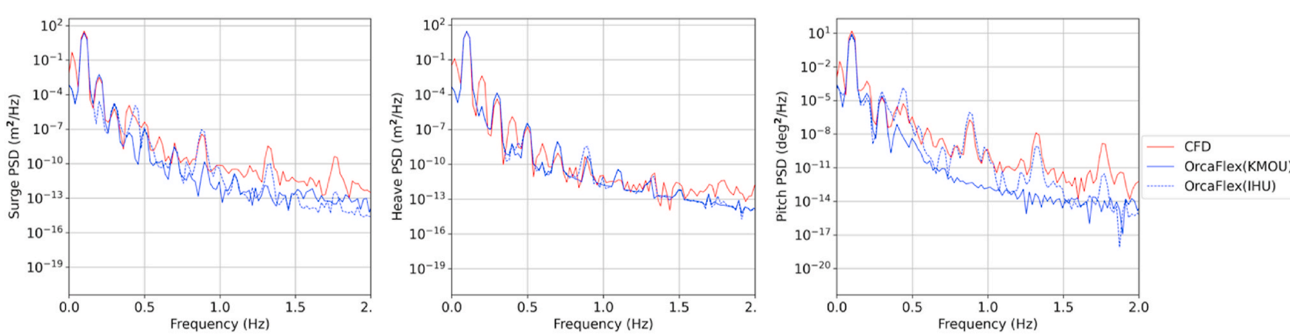


**Fig. 18.** FOWT simulation results power spectral densities.

**Table 17**
Different fidelity tools result of the fully-coupled simulation (heave, pitch, and surge displacement).

| Parameters | | OrcaFlex (KMOU) | Orcaflex (IHU) | CFD |
|---|---|---|---|---|
| Surge | Avg. [m] | −24.71 | −24.57 | −29.78 |
| | Avg. error [%] | 17.03% | 17.50% | – |
| Heave | Avg. [m] | 0.84 | 0.82 | 0.83 |
| | Avg. error [%] | 1.18% | 0.88% | – |
| Pitch | Avg. [m] | −3.78 | −3.79 | −2.71 |
| | Avg. error [%] | 28.31% | 28.53% | – |

response, except for a slightly different phase difference from CFD for heave and pitch acceleration response.

Fig. 21 shows the results of total tension on the mooring fairlead connected to the platform over time. First, examining the load on the mooring line (M1) that experiences the highest load un-der the environmental conditions, the average load response of the fairlead confirmed in OrcaFlex was about 24% lower than that of CFD without considering the load due to current. In terms of response amplitude, CFD showed a load response with a single frequency, but OrcaFlex showed a load response with multiple frequencies. Generally, the motion response due to regular waves appears to have a similar single period as the regular wave, and in such monotonous motion, the load response acting on the fairlead of the mooring line connected to the platform also applies force as if it had a single frequency. As a result, a monotonous load response appeared in Mooring line-1 in CFD. However, the reason why OrcaFlex showed a response with multiple frequencies is that the diameter of the chain that makes up the mooring line was set differently from the actual diameter to match CFD and the analysis environment. The CFD program used in this study, Star-CCM+, calculates the load on both ends of the mooring line based solely on the length and unit weight of the mooring line, as well as its axial stiffness. In contrast, OrcaFlex calculates the load on the mooring line by considering not only the length, weight, and axial stiffness but also additional characteristics such as the diameter of the mooring line and Poisson's ratio. These differences result in significant discrepancies in the analysis of the load on the mooring lines between different fidelity engineering tools. Therefore, to equalize the mooring settings, some of the characteristics of the mooring lines used in OrcaFlex were adjusted, and in the process, the diameter of the mooring lines set in OrcaFlex was reduced. As a result, a very sensitive load response to platform motion occurred.

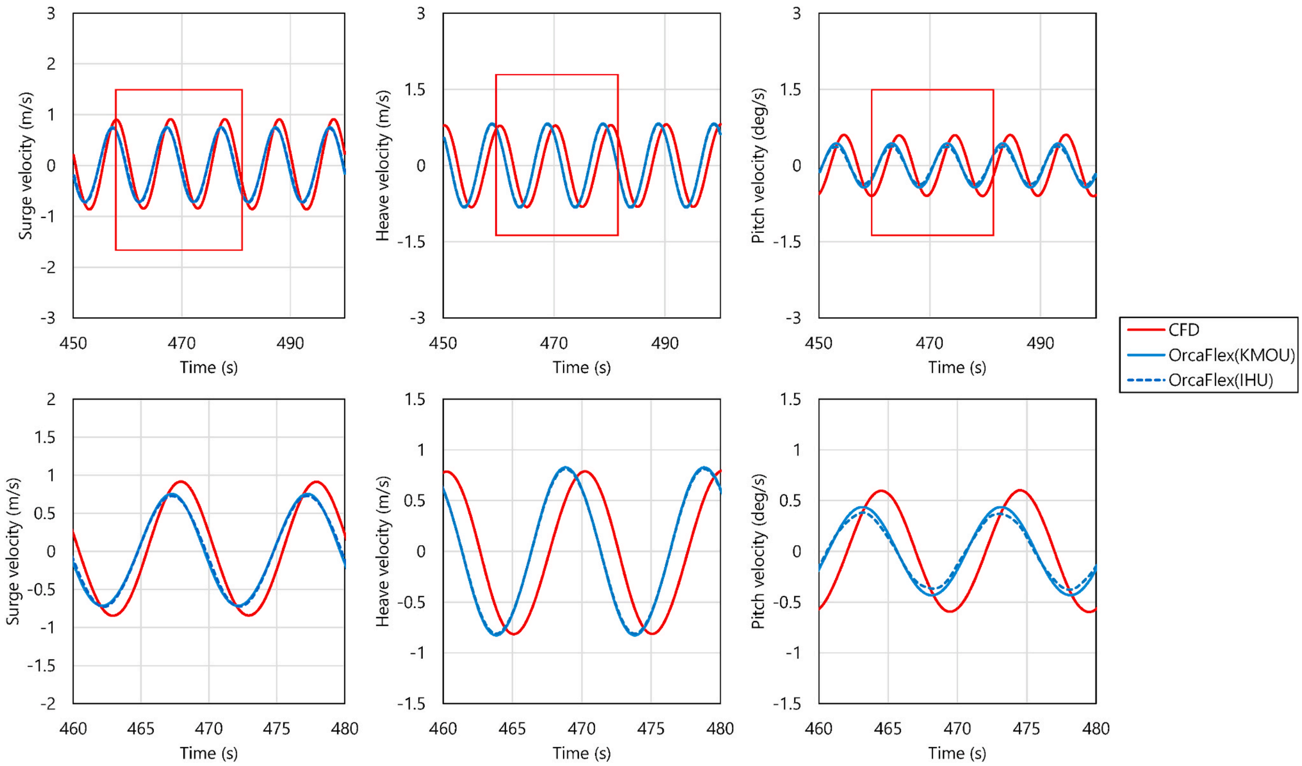


**Fig. 19.** FOWT simulation time serial velocity response result (left:have, middle:pitch, right:surge).

**Table 18**
Different fidelity tools result of the fully-coupled simulation (heave, pitch, and surge velocity).

| Parameters | | OrcaFlex (KMOU) | Orcaflex (IHU) | CFD |
|---|---|---|---|---|
| Surge velocity | Avg. [m/s] | 0.47 | 0.46 | 0.56 |
| | Avg. error [%] | 16.64% | 17.72% | – |
| Heave velocity | Avg. [m/s] | 0.53 | 0.51 | 0.51 |
| | Avg. error [%] | 2.29% | 0.19% | – |
| Pitch angular velocity | Avg. [m/s] | 0.28 | 0.24 | 0.38 |
| | Avg. error [%] | 27.03% | 37.36% | – |

Looking at the average load error of the middle-fidelity engineering tool of M2 and M3 in Table 20, it was confirmed to be quite similar to CFD within a maximum of 2%. Unlike M1, a monotonous load response similar to having a single period appeared. Since the environmental load acts in the direction where the mooring line M1 is located, the load acting on M2 and M3 is influenced more by pitch and heave responses than surge response. Comparing it with the platform motion response, it can be confirmed that the load amplitude response of M2 and M3 is influenced more by pitch than heave through the phase of the load.

## 6. Conclusion

In this study, we used high-fidelity engineering tool to investigate the motion and load response of 10 MW FOWT, for which accurate viscous effect application is challenging, and the error is analyzed by comparing the results with those obtained using middle-fidelity engineering tool. The simulation was performed using the middle fidelity engineering tool, OrcaFlex and the high-fidelity engineering tool, CFD for a FOWT (Floating Offshore Wind Turbine) including the DTU-10MW turbine, newly designed platform and tower, and mooring system. The simulation was verified by comparing the load response with the simulation performed by other institutions based on the CFD conducted as an experimental replacement, and the results are as follows:

- There is a maximum error of approximately 15% in the turbine's torque and thrust.
- The system motion response had an error of about 1% for heave, but 17% for surge and 28% for pitch.
- The load or error on the mooring system was most significant at M1 located in the same direction as the environmental load, with a maximum error of 24%.

Thrust acting on the turbine is one of the dominant factors that can cause a moment in the FOWT. The predicted thrust by CFD showed low average response and high response amplitude, but the average pitch response was about 1 m lower in CFD. IHU and KMOU thrust results showed about 4% difference, but the pitch average response was almost the same in both institutions Therefore, it was concluded that the platform motion response error in this analysis is due to the relatively lower precision of the hydrodynamic analysis of the FOWT, where general viscous effects are not applied, rather than the error in turbine performance prediction. Furthermore, the errors of the middle-fidelity engineering tool and the high-fidelity engineering tool analyzed in the mooring system also increased due to the load application of the current, and in addition, the difference in load response results of the mooring system was due to the difference in the way the mooring system was constructed and analyzed in the program.

In the case of middle-fidelity engineering tools, users need to configure the settings more specifically than with high-fidelity engineering tools to perform simulations. This can lead to different simulation results due to differences in user settings. In this study, during the middle-fidelity engineering tool interpretation configuration process, a discrepancy occurred as IHU set a platform weight about 3% heavier than the design. This led to differences in platform weight, z-direction weight center, and moment of inertia values. As a result, the maximum and minimum values of heave differed by the offset weight center displacement, and pitch also had discrepancies in the maximum and minimum values, although the differences were minimal. For turbines, there were some differences in the conversion process required to apply

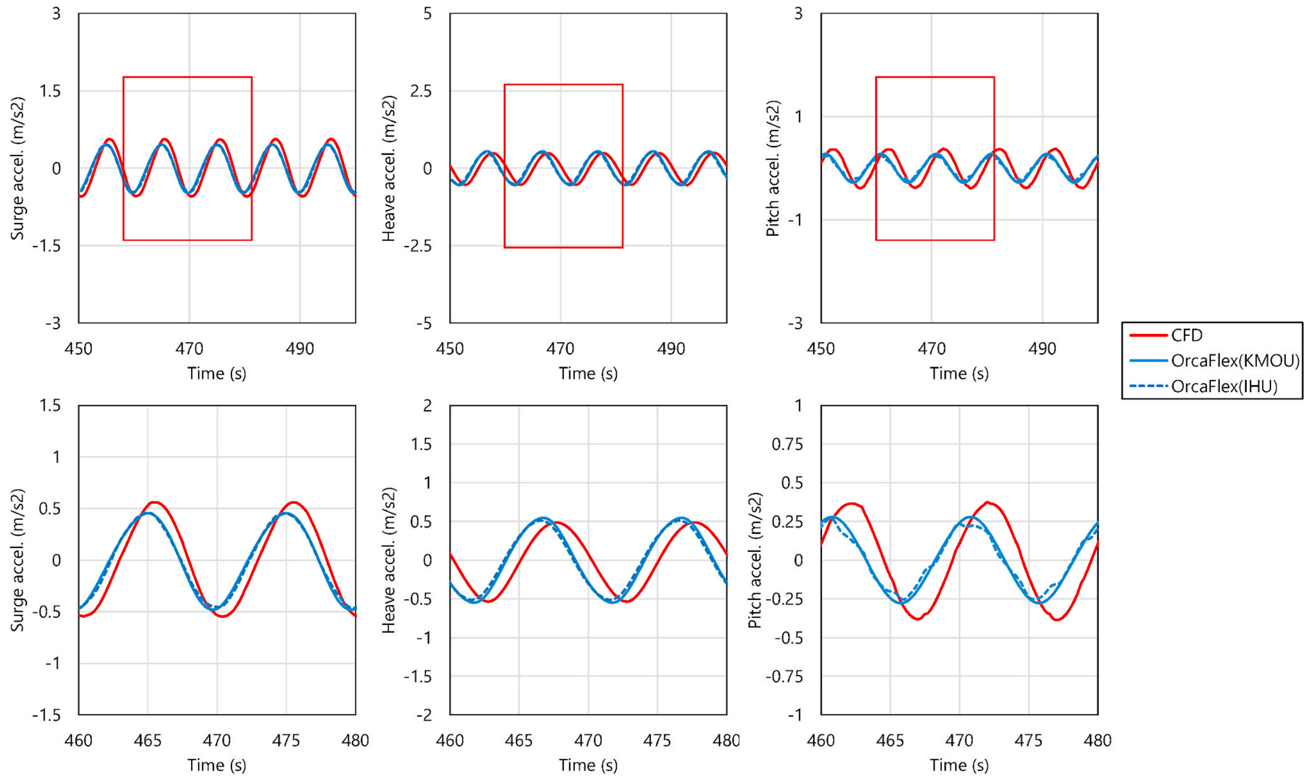


**Fig. 20.** FOWT simulation time serial acceleration response result (left:have, middle:pitch, right:surge).

**Table 19**
Different fidelity tools result of the fully-coupled simulation (heave, pitch, and surge acceleration).

| Parameters | | OrcaFlex (KMOU) | Orcaflex (IHU) | CFD |
|---|---|---|---|---|
| Surge acceleration | Avg. [$m/s^2$] | 0.47 | 0.46 | 0.56 |
| | Avg. error [%] | 16.64% | 17.72% | – |
| Heave acceleration | Avg. [$m/s^2$] | 0.53 | 0.51 | 0.51 |
| | Avg. error [%] | 2.29% | 0.19% | – |
| Pitch angular acceleration | Avg. [$m/s^2$] | 0.28 | 0.24 | 0.38 |
| | Avg. error [%] | 27.03% | 37.36% | – |

the provided turbine data to OrcaFlex, resulting in an error of approximately 4–10% in the maximum and minimum values of torque and thrust. Despite these errors, identical results were obtained for surge motion responses and tension load responses, excluding the responses mentioned above. It was determined that small weight errors in the platform weight settings influenced the average heave value, and other configuration differences in the turbine affected performance. However, the errors that occurred within this range had little impact on the surge motion response and loads acting on the mooring lines.

In this analysis, compared to previous research, we integrated and analyzed the components that make up the FOWT instead of analyzing them individually. This approach enabled us to identify the correlation between external loads on each part and their effects on the system. Furthermore, several previous studies used the simple 5 MW OC4 model, where all parts can be modeled as a cylinder. However, in this study, we used a floating body with a rectangular-shaped lower pontoon, which has a width smaller than the diameter of the column located outside, resulting in complex fluid flow on the floater's surface. This made it difficult to set generalized values for the viscous effect. Consequently, by analyzing a floater with an unstructured shape using potential flow-based analysis tools in this study and comparing the results with CFD, we can expect new insights and undiscovered results that can contribute to the development of research in this field.

Although there was some error in the load acting on the mooring line due to reflecting different line characteristics from the actual condition to match the CFD and analysis environmental conditions, it was confirmed that the overall error rate in the middle-fidelity engineering tool, including the turbine performance, floating body motion response, and mooring system load response, was reliable through comparison with CFD, which was not applied with the current load. Although this study performed analysis under extreme environmental conditions, it was conducted using regular waves rather than irregular waves. Therefore, the current research has a limitation that there may be larger errors in wave with different frequencies in the middle-fidelity engineering tool. In addition, while the CFD considered the current load on the floater due to wind-induced currents, the potential flow-based analysis tool did not take into consideration the current load induced by wind-induced currents. Moreover, the newly designed floater was only used as a reference for error analysis with CFD. Therefore, additional reduced-scale experiments on the newly designed floater are necessary for validating the CFD results used in this study. For the next study, it is necessary to conduct experiments and additional analysis to utilize the floater for research purposes in the field of FOWT, as in previous studies using the DeepCwind floater, and to provide information to utilize the data obtained from it. Furthermore, it is necessary to perform simulations in the wave frequency range with varying frequencies, considering the current induced by wind, in the CFD to analyze the error rate of the overall high-fidelity engineering tool, and to study effective and practical methods of applying the viscosity effect to reduce the error rate.

## CRediT authorship contribution statement

**Ho-Seong Yang:** Conceptualization, Methodology, Software, Investigation, Visualization, Writing – review & editingWriting - review & editing. **Watchara Tongphong:** Software, Validation. **Alkhabbaz Ali:** Software, Visualization, Investigation. **Young-Ho Lee:** Supervision.

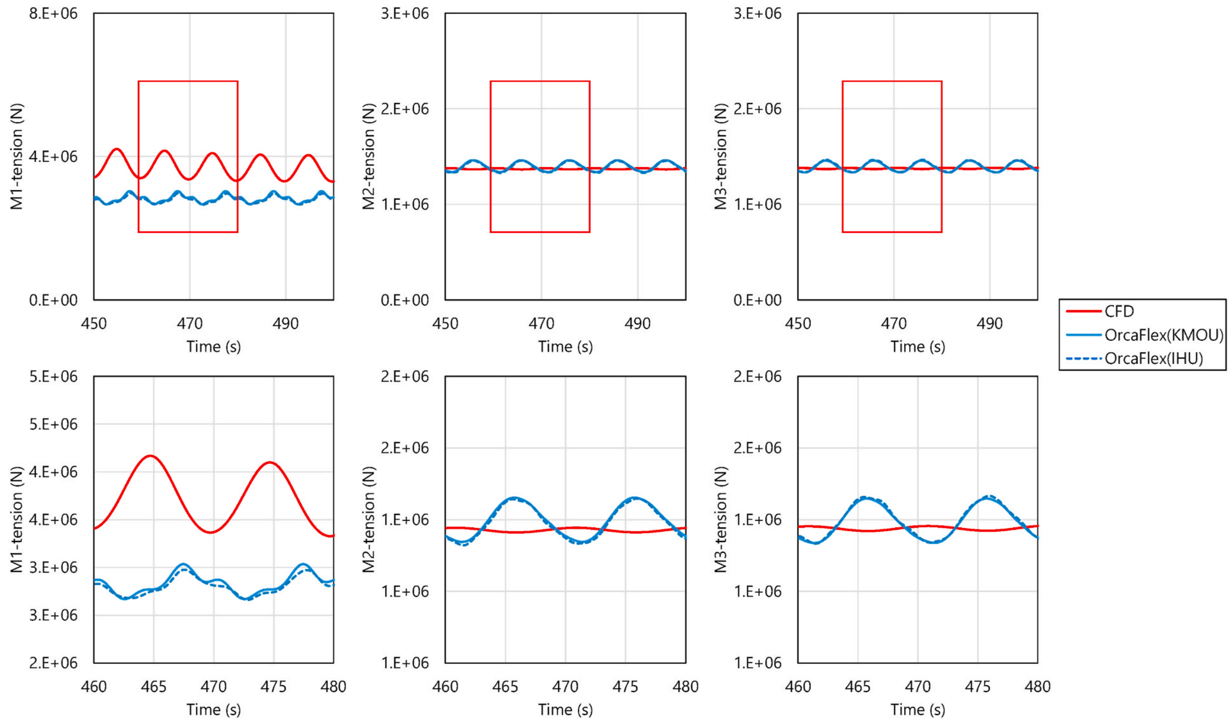


**Fig. 21.** FOWT simulation time serial mooring tension result (left:have, middle:pitch, right:surge).

**Table 20**
Different fidelity tools result of the fully-coupled simulation (mooring line fairlead total tension).

| Parameters | | OrcaFlex (KMOU) | Orcaflex (IHU) | CFD |
|---|---|---|---|---|
| M1 tension | Avg. [N] | 2,831,777 | 2,801,832 | 3,711,498 |
| | Avg. error [%] | 23.70% | 24.51% | – |
| M2 tension | Avg. [N] | 1,397,475 | 1,391,829 | 1,364,357 |
| | Avg. error [%] | 1.93% | 1.51% | – |
| M3 tension | Avg. [N] | 1,394,241 | 1,397,842 | 1,375,944 |
| | Avg. error [%] | 1.33% | 1.59% | – |

## Declaration of competing interest

The authors declare that they have no known competing financial interests or personal relationships that could have appeared to influence the work reported in this paper.

## Data availability

Data will be made available on request.

## Acknowledgements

This research was supported by Korea Institute of Energy Technology Evaluation and Planning (KETEP) grant funded by the Korean government (MOTIE) (20213000000030)—Development of disconnectable mooring system for A MW class floating offshore wind turbine.

## References

Ahlström, A., 2006. Aeroelastic Simulation of Wind Tur- Bine Dynamics.
Bak, C., Zahle, F., Bitsche, R., Yde, T.K.A., Henriksen, L.C., Natarajan, A., Hansen, M.H., 2013. Description of the DTU 10 MW Reference Wind Turbine (Roskilde, DK).
Bayati, I., Gueydon, S., Belloli, M., 2015. Study of the effect of water depth on potential flow solution of the OC4 semisubmersible floating offshore wind turbine. Energy Proc. 80, 168–176.
Bazilevs, Y., Hsu, M., Akkerman, I., Wright, S., Takizawa, K., Henicke, B., Spielman, T., Tezduyar, T.E., et al., 2011. 3D simulation of wind turbine rotors at full scale. Part I: geometry modeling and aerodynamics. Int. J. Numer. Methods Fluid. 65, 207–235.
Benitz, M.A., Schmidt, D.P., Lackner, M.A., Stewart, G.M., Jonkman, J., Robertson, A., 2014. Comparison of hydrodynamic load predictions between reduced or- der Engineering models and computational fluid dynamics for the OC4-DeepCwind semi-submersible. Ocean Renewable Energy 9.
Benitz, M.A., Schmidt, D.P., Lackner, M.A., Stewart, G.M., Jonkman, J., Robertson, A., 2015. Validation of hydrodynamic load models using CFD for the OC4-DeepCwind semisubmersible. Ocean Renew- able Energy 9.
CD-ADAPCO, 2020. STAR-CCM+ User Guide.
Glauert, H., 1926. A general theory of the autogyro. In: A General Theory of the Autogyro, Ed. others.
GWEC, 2021. Global Wind Report 2021.
Hall, M., Goupee, A., 2015. Validation of a lumped-mass mooring line model with DeepCwind semisubmersible model test data. Ocean. Eng.
Hansen, M.O.L., Sørensen, J.N., Voutsinas, S., Sørensen, N., Madsen, H.A., 2006. State of the art in wind turbine aerodynamics and aeroelasticity. Prog. Aero. Sci. 42, 285–330.
Hsu, M., Akkerman, I., Bazilevs, Y., 2014. In: Finite Element Simulation of Wind Turbine Aerodynamics: Validation Study Using NREL Phase VI Experiment, vol. 17 (Chichester, England).
IEA, 2022. Renewable Energy Market Update.
IRENA, 2021. Renewable Energy Statistics 2021.
Krogstad, P., Eriksen, P.E., 2013. Blind test" calculations of the performance and wake development for a model wind turbine. Renew. Energy 50, 325–333.
Ledru, R., Cunff, C.L., Heurtier, J., Perdrizet, T., Poirette, Y., 2014. Influence of hydrodynamic modeling assumptions on floating wind turbine behaviour. Ocean Renewable Energy 9.
Leimeister, M., Kolios, A., Collu, M., 2018. Critical review of floating support structures for offshore wind farm deployment. J. Phys.: Conf. Ser.
Luna, R.B.D., Marten, D., Barlas, T., Horcas, S.G., Ramos-García, N., Li, A., Paschereit, C. O., 2022. Comparison of different fidelity aerodynamic solvers on the IEA 10 MW turbine including novel tip extension geometries. J. Phys. 32002–32002.
Mihet-Popa, L., Blaabjerg, F., Boldea, I., 2004. Wind turbine Generator modeling and Simulation where ro- tational speed is the controlled variable. TIA 40, 3–10.
Moriarty, P.J., Hansen, A.C., 2005. Aerodyn Theory Manual.
Ohmori, T., 1998. Finite-volume simulation of flows about a ship in maneuvering motion. J. Mar. Sci. Technol. 3, 82–93.
Ortolani, A., Persico, G., Drofelnik, J., Jackson, A., Campobasso, M.S., 2020. Cross-comparative analysis of loads and power of pitching floating offshore wind turbine rotors using frequency-domain Navier-Stokes CFD and blade element momentum theory. J. Phys. Conf. 1618, 52016–52016.
Pegalajar-Jurado, A., Bredmose, H., 2019. Reproduction of Slow-Drift Motions of a Floating Wind Turbine Using Second-Order Hydrodynamics and Operational Modal Analysis.
Robertson, A., Jonkman, J., Masciola, M., Song, H., Goupee, A., Coulling, A., Luan, C., 2014a. Definition of the Semisubmersible Floating System for Phase II of OC4.

Robertson, A., Jonkman, J., Vorpahl, F., Popko, W., Qvist, J., Frøyd, L., Chen, X., Azcona, J., Uzunoglu, E., Guedes Soares, C., Luan, C., Yutong, H., Pengcheng, F., Yde, A., Larsen, T., Nichols, J., Buils, R., Lei, L., Nygaard, T.A., Manolas, D., Heege, A., Vatne, S.R., Ormberg, H., Duarte, T., Godreau, C., Hansen, H.F., Nielsen, A.W., Riber, H., Le Cunff, C., Beyer, F., Yamaguchi, A., Jung, K.J., Shin, H., Shi, W., Park, H., Alves, M., Guérinel, M., 2014b. Offshore code comparison collaboration continuation within IEA wind task 30: phase II results regarding a floating semisubmersible wind system. Ocean Renewable Energy 9B.

Robertson, A.N., Wendt, F., Jonkman, J.M., Popko, W., Dagher, H., Gueydon, S., Qvist, J., Vittori, F., Az- cona, J., Uzunoglu, E., Soares, C.G., Harries, R., Yde, A., Galinos, C., Hermans, K., De Vaal, J.B., Bozonnet, P., Bouy, L., Bayati, I., Bergua, R., Galvan, J., Mendikoa, I., Sanchez, C.B., Shin, H., Oh, S., Molins, C., Debruyne, Y., et al., 2017. OC5 Project Phase II: Validation of Global Loads of the DeepCwind Floating Semisubmersible Wind Turbine.

Robertson, A.N., Gueydon, S., Bachynski, E., Wang, L., Jonkman, J., Alarcón, D., Amet, E., Beardsell, A., Bon- net, P., Boudet, B., Brun, C., Chen, Z., Féron, M., Forbush, D., Galinos, C., Galvan, J., Gilbert, P., Gómez, J., Harnois, V., Haudin, F., Hu, Z., Dreff, J.L., Leimeis- ter, M., Lemmer, F., Li, H., Mckinnon, G., Mendikoa, I., Moghtadaei, A., Netzband, S., Oh, S., Pegalajar- Jurado, A., Nguyen, M.Q., Ruehl, K., Schünemann, P., Shi, W., Shin, H., Si, Y., Surmont, F., Trubat, P., Qwist, J., Wohlfahrt-Laymann, S., et al., 2020. OC6 Phase I: investigating the underprediction of low- frequency hydrodynamic loads and responses of a float- ing wind turbine. J. Phys. Conf. 1618, 32033–32033.

Shabana, A.A., 2001. Computational dynamics. In: Computational Dynamics, Ed. John Wiley & Sons. others.

Tran, T.T., Kim, D., 2015. The coupled dynamic response computation for a semi-submersible platform of floating offshore wind turbine. J. Wind Eng. Ind. Aerod. 147, 104–119.

Tran, T.T., Kim, D., 2018. A CFD study of coupled aerodynamic-hydrodynamic loads on a semisubmersible floating offshore wind turbine. Wind Energy 21, 70–85.

Vorpahl, et al., 2013. Offshore wind turbine environment, loads, simulation, and design. Wiley interdisciplinary reviews. Energy and environment 2, 548–570.

Wang, Q., Zhou, H., Wan, D., et al., 2012. Numerical simulation of wind turbine blade-tower interaction. J. Mar. Sci. Appl. 11, 321–327.

Wang, L., Robertson, A., Jonkman, J., Yu, Y., Koop, A., Borràs Nadal, A., Li, H., Bachynski-Polić, E., Pinguet, R., Shi, W., Zeng, X., Zhou, Y., Xiao, Q., Kumar, R., Sarlak, H., Ransley, E., Brown, S., Hann, M., Netzband, S., Wermbter, M., Méndez López, B., 2021. OC6 Phase Ib: validation of the CFD predictions of difference-frequency wave excitation on a FOWT semisubmersible. Ocean. Eng. 241, 110026.

Wu, Y., Porté-Agel, F., 2011. Large-eddy simulation of wind-turbine wakes: evaluation of turbine parametrisations. Boundary-Layer Meteorol. 138, 345–366.

Yang, H., Shen, W., Xu, H., Hong, Z., Liu, C., 2014. Pre- diction of the wind turbine performance by using BEM with airfoil data extracted from CFD. Renew. Energy 70, 107–115.

Zhou, Y., Xiao, Q., Peyrard, C., Pan, G., et al., 2021. Assessing focused wave applicability on a coupled aero- hydro-mooring FOWT system using CFD approach. Ocean. Eng. 109987–109987.